Hybrid strangeon stars

Chen Zhang[1,*] Yong Gao[2,3,4,†] Cheng-Jun Xia[5,‡] and Renxin Xu[3,4,§]

[1]*The HKUST Jockey Club Institute for Advanced Study, The Hong Kong University of Science and Technology, Hong Kong SAR, People's Republic of China*
[2]*Max-Planck-Institut für Gravitationsphysik (Albert-Einstein-Institut), Am Mühlenberg 1, D-14476 Potsdam-Golm, Germany*
[3]*Department of Astronomy, School of Physics, Peking University, Beijing 100871, China*
[4]*Kavli Institute for Astronomy and Astrophysics, Peking University, Beijing 100871, China*
[5]*Center for Gravitation and Cosmology, College of Physical Science and Technology, Yangzhou University, Yangzhou 225009, China*

It was conjectured that the basic units of the ground state of bulk strong matter may be strange-clusters called strangeons, and they can form self-bound strangeon stars that are highly compact. Strangeon stars can develop a strange quark matter (SQM) core at high densities, particularly in the color-flavor-locking phase, yielding a branch of hybrid strangeon stars. We explore the stellar structure and astrophysical implications of hybrid strangeon stars. We find that hybrid strangeon stars can meet various astrophysical constraints on pulsar masses, radii, and tidal deformabilities. Finally, we show that the strangeon-SQM mixed phase is not preferred if the charge-neutrality condition is imposed at the strangeon-SQM transition region.

I. INTRODUCTION

The detection of gravitational waves (GWs) from the coalescence of compact binaries by LIGO/Virgo collaborations [1–7] has greatly improved our knowledge of black holes and compact stars. They offer unique opportunities to probe unconventional QCD matter phases, such as quark matter and strangeon matter.

Quark matter (QM), a state comprised of deconfined free-flowing quarks, can possibly exist inside the neutron star core (i.e., conventional hybrid stars [8,9]). If they are stable at zero pressure, either in form of strange quark matter (SQM) [10–13] or up-down quark matter (udQM) [14], they can constitute an entire quark star [15–27] or the crust (i.e., inverted hybrid stars [28]), both with potentially distinct astrophysical implications [29–43]. Effects from QCD interactions such as color-superconductivity and perturbative QCD (pQCD) corrections can help quark stars meet various astrophysical constraints [44–46]. Generally, it is expected that at very high densities quark matter should be in the color-flavor-locking phase (CFL), where u, d, s quarks form cooper pairs antisymmetrically in color-flavor

space with equal fractions by the attractive one-gluon exchange channel, providing a lowered energy state.

Strangeon matter (SM) is similar to strange quark matter where both are composed of a nearly equal number of u, d, s quarks [47–50]. However, strangeon matter has quarks localized as clusters in a globally solid state due to the large masses of and the strong coupling between strangeons. Strangeon stars [47–56] composed of strangeon matter have an intrinsic stiff equation of state (EOS) and large compactness, and they had already been proposed to support massive pulsars ($\gtrsim 2M_\odot$ [50]) before the announcement of the first massive pulsar PSR J1614-2230 [57]. Recently, we have shown that all strangeon stars are compact enough to feature a photonsphere that is essential to the generation of GW echoes [58].

The transition from strangeon matter to strange quark matter is likely to occur, considering such "deconfinement" originates from a shrinking of strangeon lattice spacing as density or pressure increases so that the lattice constant becomes smaller than the radius of individual quark bags, as described by the linked bag model in Ref. [49]. This gives rise to a new type of stellar objects, the *hybrid strangeon stars*, consisting of a strangeon crust and a strange quark matter core. Pure strangeon stars can form from neutron stars absorbing strangeon nuggets, or quantum nucleation in the interior. If SQM is more stable than SM at some density, then the same process can take place and form hybrid strangeon stars directly or through the

*iasczhang@ust.hk
†gaoyong.physics@pku.edu.cn
‡cjxia@yzu.edu.cn
§r.x.xu@pku.edu.cn

123031-1

SQM quantum nucleation inside strangeon stars. Such first-order phase transition needs the center pressure to be larger than some critical value at the corresponding central chemical potential. Such lift of center pressure beyond critical point can happen from spin-down, accretion, or merger of strangeon stars.

As for the organization of this paper, we first introduce the EOSs of SM and SQM, and constrain the EOS parameters from the stability considerations. Then, with Maxwell constructions where a sharp interface is assumed, we solve the hybrid stellar structures and study their compatibility with astrophysical constraints. Finally, we explore the possibility of mixed phase (Gibbs construction) where the transition region is with mixed SM and SQM rather than a sharp interface.

II. EQUATIONS OF STATES

For the quark matter sector, we adopt the unified treatment of interacting quark matter that recently developed in [46] and later applied in several studies [59–65].

Referring to [46], we first rewrite the thermodynamic potential Ω of the superconducting quark matter [8,66–69] in a general form with the pQCD correction [70] included:

$$\Omega = -\frac{\xi_4}{4\pi^2}\mu^4 + \frac{\xi_4(1-a_4)}{4\pi^2}\mu^4$$
$$-\frac{\xi_{2a}\Delta^2 - \xi_{2b}m_s^2}{\pi^2}\mu^2 - \frac{\mu_e^4}{12\pi^2} + B, \quad (1)$$

where μ and μ_e are the respective average quark and electron chemical potentials. The first term represents the unpaired free quark gas contribution. The second term with $(1-a_4)$ represents the pQCD contribution from one-gluon exchange for gluon interaction to $O(\alpha_s^2)$ order. To phenomenologically account for higher-order contributions, we can vary a_4 from $a_4 = 1$, corresponding to a vanishing pQCD correction, to very small values where these corrections become large [8,45,70]. The term with m_s accounts for the correction from the finite strange quark mass if applicable, where $m_s = 95 \pm 5$ MeV [71], and we choose $m_s = 95$ MeV as its benchmark value. The term with the gap parameter Δ represents the contribution from color superconductivity. $(\xi_4, \xi_{2a}, \xi_{2b})$ represents different state of color-superconducting phases. B is the effective bag constant that accounts for the nonperturbative contribution from the QCD vacuum.

The corresponding equation of state was derived in Ref. [46]:

$$P = \frac{1}{3}(\rho - 4B) + \frac{4\lambda^2}{9\pi^2}\left(-1 + \text{sgn}(\lambda)\sqrt{1 + 3\pi^2\frac{(\rho - B)}{\lambda^2}}\right), \quad (2)$$

where

$$\lambda = \frac{\xi_{2a}\Delta^2 - \xi_{2b}m_s^2}{\sqrt{\xi_4 a_4}}. \quad (3)$$

Note that $\text{sgn}(\lambda)$ represents the sign of λ. The chemical potential (per baryon number) has the following form:

$$\mu_{\text{QM}} = \frac{3\sqrt{2}}{(a_4\xi_4)^{1/4}}\sqrt{[(P+B)\pi^2 + \lambda^2]^{1/2} - \lambda}. \quad (4)$$

Taking the zero pressure limit of μ_{QM}, we obtain the energy per baryon number, which can be converted into the following form:

$$\left(\frac{E}{A}\right)_{\text{QM}} = \frac{3\sqrt{2}\pi}{(\xi_4 a_4)^{1/4}}\frac{B^{1/4}}{\sqrt{(\lambda^2/B + \pi^2)^{1/2} + \lambda/\sqrt{B}}}, \quad (5)$$

where we see a larger λ lowers the energy as expected.

We have examined that hybrid strangeon star with a core of unpaired strange quark matter ($\Delta = 0$) cannot support $2M_\odot$ while retaining radial stability that requires $\partial M/\partial P_c > 0$. This is not a surprise considering strangeon EOS is much stiffer than that of unpaired SQM, and a transition to a much softer EOS is likely to induce radial instabilities due to insufficient degenerate pressure to resist the gravitational pulling. We can thus stabilize the hybrid strangeon stars by introducing color-super-conductivity effects to stiffen the SQM EOS.[1] Therefore, in the following discussions, we specify the SQM phase to be CFL ($\xi_4 = 3, \xi_{2a} = 3, \xi_{2b} = 3/4$), considering the shared flavor composition and the fact that color superconductivity stiffens the EOSs. Besides, we set $a_4 = 1$ (no extra QCD corrections) for simplicity.

Following previous studies [47–56], we assume the interaction potential between two strangeons is described by the Lennard-Jones potential [74]:

$$U(r) = 4\epsilon\left[\left(\frac{\sigma}{r}\right)^{12} - \left(\frac{\sigma}{r}\right)^6\right], \quad (6)$$

where r is the distance between two strangeons, and σ is the distance when $U(r) = 0$. The parameter ϵ describes the depth of the interaction potential between strangeons.

---

[1]Such instabilities can also be cured by considering the scenario of slow SM-SQM conversions (with respect to radial-oscillation timescale) [72,73]. Considering both SM and CFL have the three-flavor symmetry, we expect that the surface tension of SM-SQM is not large, thus the conversion is likely to be fast and correspondingly the stability criteria retains to be $\partial M/\partial P_c > 0$, i.e., the star mass increases with center pressure.

A larger ϵ will then indicate a larger repulsive force at short range and thus maps to a stiffer EOS.

The mass density ρ and pressure p of zero-temperature dense matter composed of strangeons derived from the Lennard-Jones potential [50] reads

$$\rho = 2\epsilon(A_{12}\sigma^{12}n^5 - A_6\sigma^6 n^3) + nN_q m_q, \qquad (7)$$

$$P = n^2 \frac{\mathrm{d}(\rho/n)}{\mathrm{d}n} = 4\epsilon(2A_{12}\sigma^{12}n^5 - A_6\sigma^6 n^3), \qquad (8)$$

where $A_{12} = 6.2$, $A_6 = 8.4$, and n is the number density of strangeons. $N_q m_q$ is the mass of a strangeon with N_q being the number of quarks in a strangeon and m_q being the average constituent quark mass. The contributions from degenerate electrons and vibrations of the lattice are neglected due to their expected smallness.

At the surface of strangeon stars, the pressure becomes zero, and we obtain the surface number density of strangeons as $[A_6/(2A_{12}\sigma^6)]^{1/2}$. For convenience, it is transformed into baryon number density, i.e.,

$$n_s = \left(\frac{A_6}{2A_{12}}\right)^{1/2} \frac{N_q}{3\sigma^3}, \qquad (9)$$

so that the EOS can be rewritten into the following simpler form

$$\frac{\rho}{n_s} = \frac{a}{9}\tilde{\epsilon}\left(\frac{1}{18}\bar{n}^5 - \bar{n}^3\right) + m_q\bar{n},$$

$$\frac{P}{n_s} = \frac{2a}{9}\tilde{\epsilon}\left(\frac{1}{9}\bar{n}^5 - \bar{n}^3\right), \qquad (10)$$

where $a = A_6^2/A_{12} = 8.4^2/6.2 \approx 11.38$, $\tilde{\epsilon} = \epsilon/N_q$, and $\bar{n} = N_q n/n_s$. Note that $\bar{n} = 3$ at star surface where $P = 0$.

The chemical potential of strangeon matter can be derived via the thermodynamic relation $\mu = (\rho + P)/n$. Note that to study its crossings with μ_{QM}, one needs to further convert it to the chemical potential per baryon number

$$\mu_{\mathrm{strangeon}} = \frac{3\mu}{N_q} = 3\frac{\rho/n_s + P/n_s}{\bar{n}} = 3m_q + a\tilde{\epsilon}\left(\frac{5}{54}\bar{n}^4 - \bar{n}^2\right). \qquad (11)$$

Referring to Eq. (10), we see that both the EOS $P(\rho)$ and $\mu_B(P)$ for strangeons only depends on parameters n_s and $\tilde{\epsilon}$ with the dependence on N_q absorbed. Taking the zero pressure limit of $\mu_{\mathrm{strangeon}}$, we obtain the energy per baryon number at the bulk limit:

$$\left(\frac{E}{A}\right)_{\mathrm{strangeon}} = 3m_q - \frac{3a}{2}\tilde{\epsilon}, \qquad (12)$$

where we see that E/A has no dependence on n_s, decreases as $\tilde{\epsilon}$ increases, so that strangeon matter can be the ground state of matter at the bulk limit for a finite $\tilde{\epsilon}$. In this proof-of-concept work, we adopt $3m_q = 930$ MeV for simplicity, ensuring that, at the bulk limit, strangeon matter is always more stable than nucleon matter, since $(E/A)_{\mathrm{strangeon}} < (E/A)_{\mathrm{Fe}} = 930$ MeV, the energy per baryon number of the most stable nucleus ^{56}Fe. Requiring a positive E/A (or a non-negative ρ at zero pressure) sets a theoretical bound: $\epsilon/N_q \leq 2m_q/a \approx 54.5$ MeV.

The transition pressure or density can be determined by the crossings of their chemical potentials. A necessary condition for such chemical potential crossing is that the zero-pressure chemical potential (i.e., energy per baryon number E/A) of strangeon [Eq. (12)] is smaller than that of CFL [Eq. (5)]. We show the related parameter space as the blue-shaded bands of Fig. 1. We see that overall, the
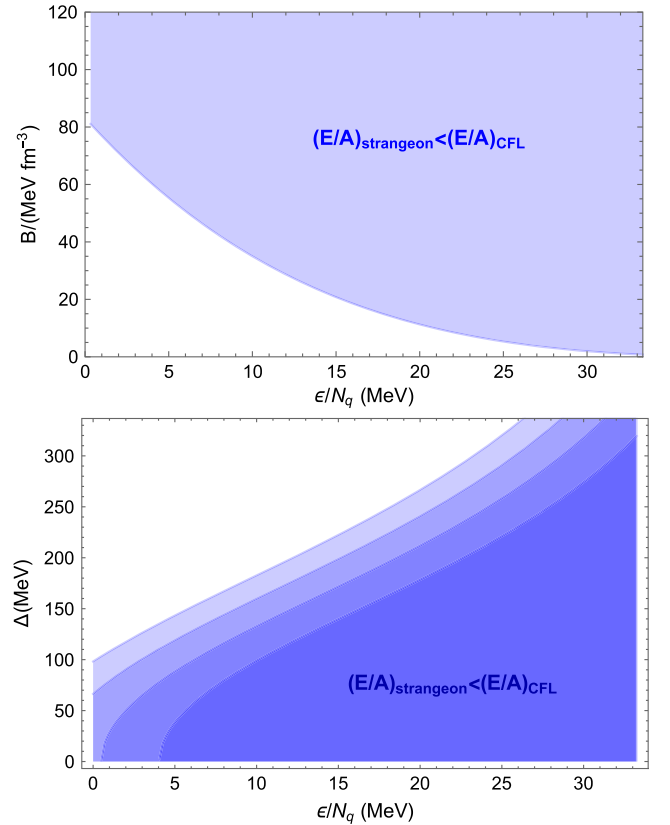

FIG. 1. Allowed parameter space (blue-shaded) for the existence of hybrid strangeon stars from stability consideration $(E/A)_{\mathrm{Strangeon}} < (E/A)_{\mathrm{CFL}}$. Top: CFL bag constant B and bottom: CFL superconductivity gap Δ versus parameter ϵ/N_q of strangeon matter. For the bottom sub-figure, the shaded region with lighter-colored contour lines represents larger bag constant, sampling $B = 60, 80, 100, 120$ MeV/fm^3 (bottom to top).

existence of such a hybrid configuration prefers a relatively stiff strangeon EOS (large $\tilde{\epsilon}$) but a relatively soft CFL phase (large B or small Δ).

On the other hand, the hybrid configuration would become radially unstable ($\partial M/\partial P_c < 0$) if the transition pressure P_{trans} is too large [9], as we have also examined explicitly. Referring to Eqs. (4) and (11), we see that the strangeon matter to SQM transition is more likely to occur at smaller P_{trans} in the case of a smaller B, a larger Δ (stiffer SQM EOS), a smaller $\tilde{\epsilon}$ (softer SM EOS) or smaller n_s. These conditions compete with those from the stability condition mentioned in the previous paragraph, constraining the allowed parameter space.

III. ASTROPHYSICAL IMPLICATIONS

The stellar structure can be solved via the Tolman-Oppenheimer-Volkoff (TOV) equation [75,76],

$$\frac{dm}{dr} = 4\pi\rho r^2,$$

$$\frac{dP}{dr} = (\rho + P)\frac{m + 4\pi P r^3}{2mr - r^2}, \qquad (13)$$

where the profiles $P(r)$ and $m(r)$ are solved as functions of the center pressure P_c. The radius R and physical mass M of the compact stars are determined by $P(R) = 0$ and $M = m(R)$, respectively. One then obtains the mass-radius relation $M(R)$ of hybrid strangeon stars by solving the TOV equations together with the EOSs of the two matter phases, where the transition point is determined by the crossing of their chemical potentials, as introduced in the last section.

To compare with gravitational wave observations, we can further compute the dimensionless tidal deformability $\Lambda = 2k_2/(3C^5)$, where $C = M/R$ is the compactness and k_2 is the Love number that characterizes the stars' response to external disturbances [77–80]. The Love number k_2 can
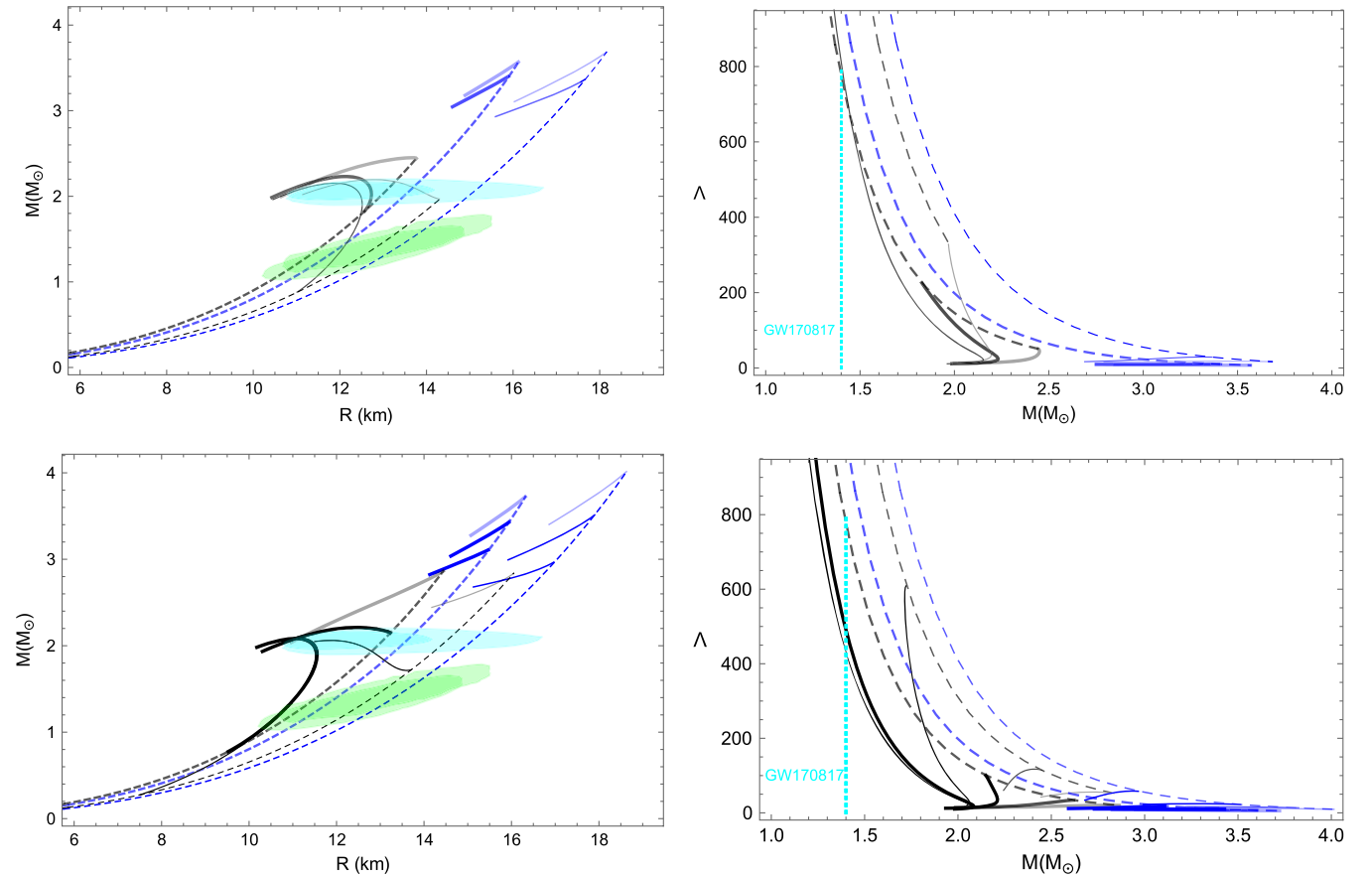

FIG. 2.   The curves M-R (left) and Λ-M (right) of hybrid strangeon stars (solid lines) with $\epsilon/N_q = 80/9 \approx 8.9$ (black), $120/9 \approx 13.3$ (blue) MeV, $n_s = 0.22$ (thin), 0.30 (thick) fm^{-3} for the strangeon composition, and $B = 60$ (top), 80 (bottom) MeV/fm^3 for the CFL composition. Lines with darker colors denote larger Δ, sampling 60, 80 MeV for top panels and 60, 100, 120 MeV for bottom panels, respectively. (no large-Δ lines in top panels due to stability constraints referring to Fig. 1.) Dashed lines are pure strangeon star configurations. Shaded regions are constraints with 90% credibility from the NICER mission PSR J0030 + 0451 (green colored) [83,84], PSR J0740 + 6620 (cyan colored) [85,86]. The cyan-dotted vertical line in the right panels denotes the GW170817's $\Lambda(1.4M_\odot) \leq 800$ constraint [4].
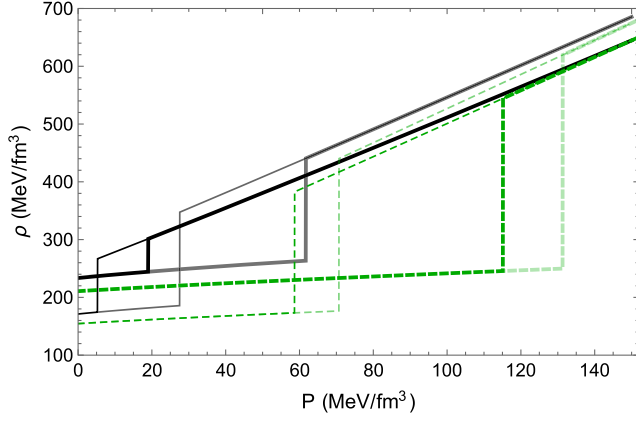
FIG. 3. The relations of $\rho(P)$ for stable hybrid strangeon stars, with $\epsilon/N_q = 80/9$ MeV, $n_s = 0.22$ (thin), 0.30 (thick) fm^{-3} for the strangeon composition, and $B = 60$ (green dashed), 80 (black solid) MeV/fm^3 for the CFL composition. Lines with darker colors denote larger Δ, sampling 60, 80 MeV for green lines and 100, 120 MeV for black lines, respectively.

TABLE I. Correlations of constraints and the EOS parameters. Plus (minus) sign means positive (negative) correlation, while the three centerdots mean no correlation.

	$\tilde{\epsilon}$	n_s	Δ	B
$(E/A)_{\text{Strangeon}} < (E/A)_{\text{CFL}}$	$+$	$\cdots$	$-$	$+$
$\partial M/\partial P_c > 0$	$-$	$-$	$+$	$-$
$M_{\text{TOV}} \gtrsim 2M_\odot$	$+$	$-$	$+$	$-$
$\Lambda_{1.4M_\odot} \leq 800$	$-$	$+$	$-$	$+$

be determined by solving a function $y(r)$ from a specific differential equation [80] and the TOV equation Eq. (13), with the boundary condition $y(0) = 2$. For hybrid configurations, the matching condition [81,82] $y(r_d^+) - y(r_d^-) = -4\pi r_d^3 \Delta\rho_d/(m(r_d) + 4\pi r_d^3 P(r_d))$ should be imposed at r_d (i.e., the core radius and the star radius), where an energy density jump $\Delta\rho_d$ occurs.

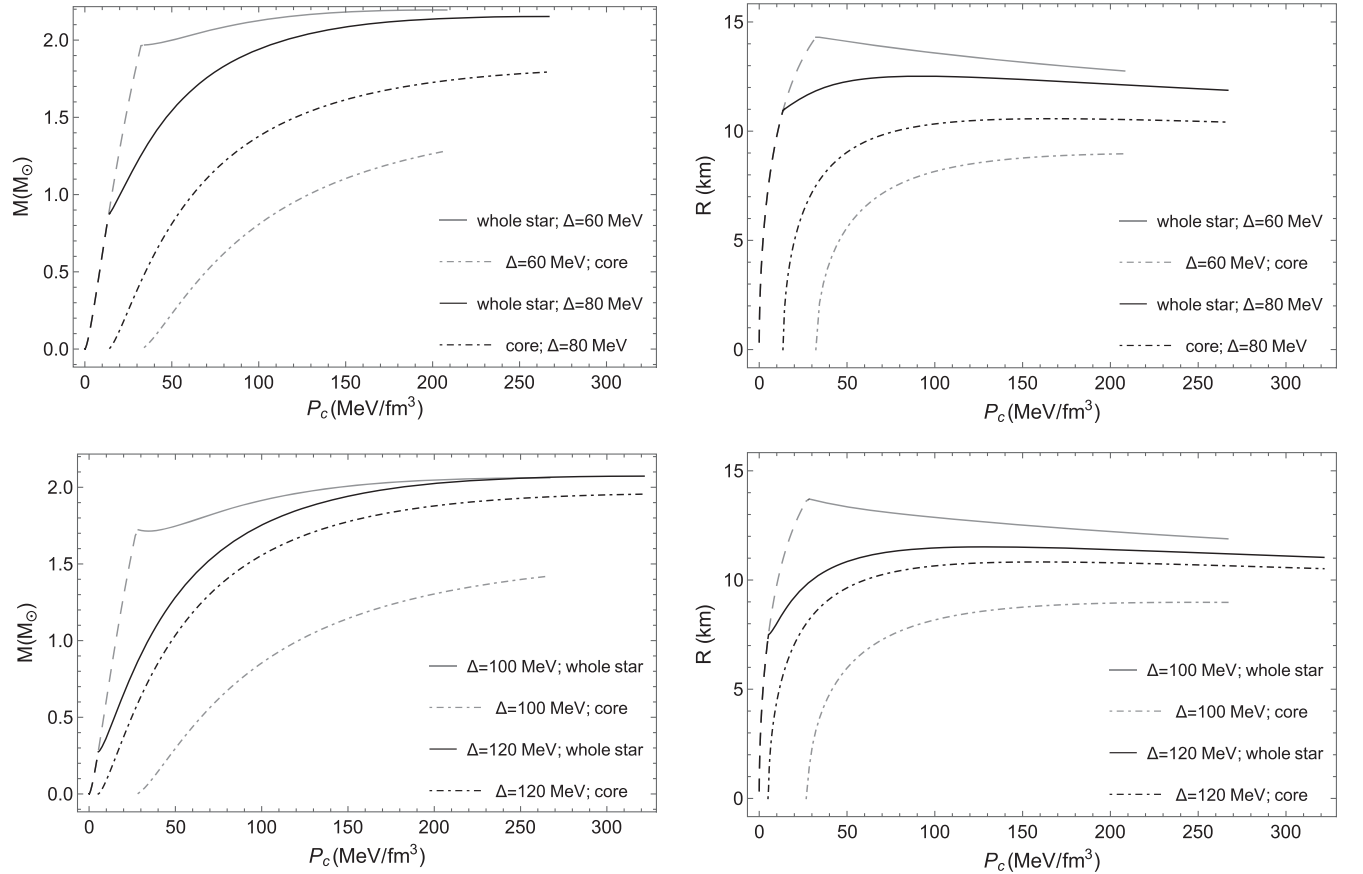For illustration, we show various benchmark TOV solutions and corresponding tidal deformabilities in Fig. 2 for

FIG. 4. Mass (left) and radius (right) versus center pressure, P_c, for hybrid strangeon stars with strangeon crusts of $\{n_s = 0.22/\text{fm}^3, \tilde{\epsilon} = 80/9 \text{ MeV}\}$, and CFL cores of $\{B = 60 \text{ MeV}/\text{fm}^3, \Delta = 60, 80 \text{ MeV}\}$ (top) and $\{B = 80 \text{ MeV}/\text{fm}^3, \Delta = 100, 120 \text{ MeV}\}$ (bottom). Darker color denotes larger Δ values. Dashed lines denote pure strangeon stars. Solid lines denote hybrid strangeon stars. The dot-dashed lines denote the CFL cores. The right ends of the solid and dot-dashed lines are truncated at the corresponding maximum mass points.

$B = 60$, 80 MeV/fm³ with $\tilde{\epsilon}$ and Δ choices satisfying $(E/A)_{\text{Strangeon}} < (E/A)_{\text{CFL}}$ (shaded bands in Fig. 1).

We see that all the benchmark examples shown in Fig. 2 satisfy NICER constraints,[2] while the GW170817 constraints ($\Lambda_{1.4M_\odot} \leq 800$) can be met by hybrid strangeon stars with $(\tilde{\epsilon}, n_s/\text{fm}^{-3}, \Delta/\text{MeV}) = (80/9, 0.22, 80)$ for $B = 60$ MeV/fm³ (upper panels), and $(\tilde{\epsilon}, n_s/\text{fm}^{-3}, \Delta/\text{MeV}) = (80/9, 0.22, 120)$, $(80/9, 0.3, 120)$ for $B = 80$ MeV/fm³ (lower panels).

The general features of correlations between constraints and parameters are summarized in Table I. For example, as the second row of Table I summarizes, hybrid strangeon stars with small $\tilde{\epsilon}$ (black lines) and n_s (thin lines), or large Δ (darker colored lines) and small B (such as upper panels) tend to be radially unstable ($\partial M/\partial P_c < 0$), which means radial stabilities require CFL to be not too soft compared to the stiffness of strangeon EOS, considering Δ and ϵ/N_q signal the stiffness of each of the two matter phases. However, we also see that the $M_{\text{TOV}} \gtrsim 2M_\odot$ constraint [57] prefers overall stiff EOSs for both two matter phases (a large $\tilde{\epsilon}$ or Δ), while GW170817 tidal deformability constraint ($\Lambda_{1.4M_\odot} \leq 800$ [4]) prefers the opposite at low center densities. These together set bounds on the allowed parameter space.

For completeness, we plot in Fig. 3 the EOSs of the branches of Fig. 2 that have stable hybrid strangeon stars. We see that the transition mass density ρ_{trans}, as determined from chemical potential crossing, is around the nuclear saturation mass density ($\rho_{\text{sat}} \approx 157$ MeV/fm³) for $n_s = 0.22/\text{fm}^3$ lines, and increases to $1.5\rho_{\text{sat}}$ for $n_s = 0.30/\text{fm}^3$ lines. The mass density jumps at the transition points vary from 100 MeV/fm³ to 370 MeV/fm³, mainly affected by the variations of parameter Δ.

To elaborate on the explicit layer structure, we dissect hybrid strangeon stars by showing the masses and radii of their CFL cores as functions of the centre pressure in Fig. 4. Here, we choose two benchmark examples of bag constant $B = 60, 80$ MeV/fm³ with different CFL gaps and a fixed strangeon phase ($n_s = 0.22/\text{fm}^3, \tilde{\epsilon} = 80/9$ MeV). We find that, as a general feature, the compact stars are pure strangeon stars at low P_c, and then develop a CFL core as P_c increases. At the maximum mass points, the strangeon crusts have widths of 1–5 km and masses of $0.1 \sim 1M_\odot$, where a smaller bag constant or a smaller Δ maps to a thicker crust. At the $M = 2M_\odot$ point, all cases map to hybrid strangeon stars, with a core of mass $1.13(1.86)M_\odot$ for $\Delta = 100(120)$ MeV case when $B = 80$ MeV/fm³, and a core of mass $0.27(1.50)M_\odot$ for $\Delta = 60(80)$ MeV case when $B = 60$ MeV/fm³. At the $M = 1.4M_\odot$ point, for $B = 60(80)$ MeV/fm³, the

$\Delta = 60(100)$ MeV case is a pure strangeon star, while the $\Delta = 80(120)$ MeV case is a hybrid strangeon star with a core of mass $0.64(1.16)M_\odot$.

IV. MIXED PHASE

A strangeon-quark mixed phase is possible around the intersurface of the strangeon crust and quark matter core, in analogy to the hadron-quark mixed phase in the conventional hybrid neutron stars.

To construct mixed phase of hybrid strangeon stars, we need $\mu_e \neq 0$, thus the strange quark matter sector should be in either the normal unpaired phase ($\Delta = 0$)[3] or the charged CFL phase [8], where s quarks no longer have an equal fraction as u, d quarks. We keep the flavor-symmetry in the strangeon sector considering its solid state with charge-neutrality being enforced, since the Compton wavelength of dilute electrons is much larger than the scale of a strangeon.

We adopt here the Gibbs construct for the mixed phase as outlined in Ref. [87]. In this case, one may achieve the charge neutrality where the pressures of both strangeon and quark matter are functions of the baryon and electron chemical potentials μ_B and μ_e. The Gibbs condition for the equilibrium between the two phases (at zero temperature) is

$$P_{\text{SnP}}(\mu_B, \mu_e) = P_{\text{QkP}}(\mu_B, \mu_e) = P_{\text{MxP}}(\mu_B, \mu_e), \quad (14)$$

where the pressure function for strangeon phase $P_{\text{SnP}}(\mu_B)$ can be inferred from Eqs. (10) and (11) with addition of background electrons $P_{\text{SnP}}(\mu_B, \mu_e) = P_{\text{SnP}}(\mu_B) + \mu_e^4/(12\pi^2)$. Besides, for quark matter phase P_{QkP} can be inferred from Eq. (1) with the identities $p = -\Omega$, $\mu = \mu_B/3$. Their intersection yields the mixed phase $P_{\text{MxP}}(\mu_B, \mu_e)$, as shown in Fig. 5.

The global charge neutrality condition reads

$$(1 - \chi)n_c^{\text{SnP}} + \chi n_c^{\text{QkP}} = 0, \quad (15)$$

where, n_c^{SnP} and n_c^{QkP} denote the total charge densities in strangeon phase and quark matter phase (either unpaired SQM or CFL) respectively, with

$$n_c^{\text{SnP}} = -n_c^e, \quad (16)$$

$$n_c^{\text{QkP}} = \frac{2}{3}n_u - \frac{1}{3}n_d - \frac{1}{3}n_s - n_c^e, \quad (17)$$

where $n_c^e = \mu_e^3/(3\pi^2)$, $n_{u,d} = \mu_{u,d}^3/\pi^2$, $n_s = (\mu_s^2 - m_s^2)^3/\pi^2$ with μ_i the quark chemical potential of flavor i. χ defines the volume fraction of the quark matter in mixed phase defined as $\chi = V_{\text{QkP}}/(V_{\text{QkP}} + V_{\text{SnP}})$.

---

[2]Note that we show the NICER x-ray constraints in the graph but neglect them in the table considering the x-ray analyses of hybrid strangeon stars may be different from those of neutron stars.

[3]As aforementioned for the sharp transition, normal strange quark matter core with a strangeon crust are not likely to be radially-stable. We expect the situation may be alleviated in the mixed phase scenario.
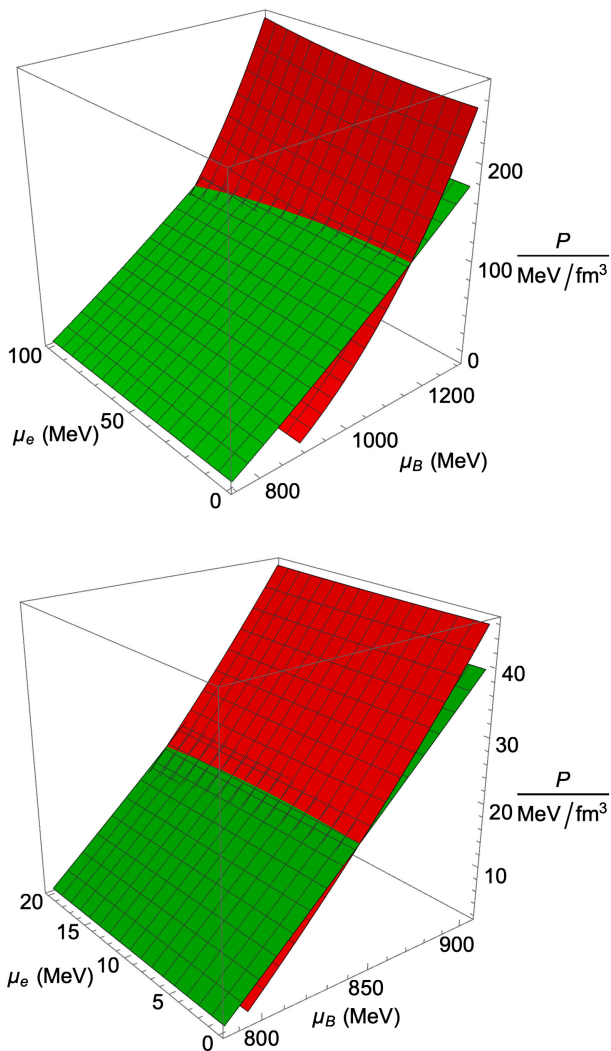
FIG. 5. Pressure is plotted as a function of μ_B and μ_e for strangeon phase (green) and strange quark matter (red) of normal unpaired (top panel) and charged CFL phase (bottom panel) of $\Delta = 100$ MeV. The mixed phase sits in the intersection of the two surfaces. For illustration, here $B = 80$ MeV/fm^3, $m_s = 95$ MeV for the SQM phase and $\epsilon/N_q = 80/9, n_s = 0.3/$fm^3 for strangeon phase.

We have examined various combinations of parameter sets for SQM in either the normal unpaired phase or CFL phase, finding that the mixed phase $P_{\mathrm{MxP}}(\mu_B, \mu_e)$ that satisfies the global charge neutrality condition only resides in a very tiny segment of the intersection line, with variations of μ_B smaller than 1 MeV range near the zero μ_e point, where μ_e lift to 6–8 MeV. Thus the mixed-phase region for hybrid strangeon stars is negligible, and all results should approximately be the same as those obtained from the Maxwell construction studied in the last section, i.e., the system is effectively reduced into one conserved charge due to the negligible contribution of electrons. As we have examined, introducing QCD corrections ($a_4 < 1$) will lift the intersecting μ_B but does not help

enlarge the charge-neutral region of the mixed phase. This matches the expectation that the flavor-symmetry breaking effects are small in both strangeon and SQM sectors, resulting in a very small μ_e and its limited variation range when considering charge neutrality.

V. SUMMARY AND DISCUSSION

We have explicitly shown the new possibility of the hybrid configuration of strangeon stars with a strange quark matter core and a thick strangeon crust. We also demonstrated their compatibility with astrophysical constraints with selected benchmark examples. It is shown that mixed phase is not preferred for hybrid strangeon stars with a CFL core.

Hybrid strangeon stars can naturally accommodate the pulsar glitch phenomena as a result of the star quakes in the thick strangeon crust [88–91], in contrast to compact stars with the crystalline color superconducting phase where glitches are a result of superfluid vortices pinned to the solid component [92–95]. The large density discontinuity at the SM-CFL intersurface (referring to Fig. 3) will induce g-mode gravitational waves from nonradial oscillations that might help differentiate hybrid strangeon stars and other types of compact stars [96–100]. Besides, the large shear modulus change and density continuities at the crust-core interface are likely to result in large and distinct crust-core interfacial modes that can also be probed by gravitational-wave observations [101,102].

As aforementioned, the conversions from strangeon matter to strange quark matter (either unpaired or CFL) is likely to be fast from intuitive expectations. However, due to the intrinsic uncertainties of the SM-SQM surface tension in nonperturbative QCD, it is not entirely impossible that the conversion is slow compared to the radial oscillation timescale, corresponding to the slow conversion scenario where branches of $\partial M/\partial P_c < 0$ can also be stable. In this case, referring to Table I, the allowed parameter space for stable hybrid strangeon stars can be enlarged. In particular, superconducting gap Δ can now have smaller values without ruining the radial stability. Similar relaxation of parameter constraints would also be possible when considering the merger remnants with extremely spinning where the unstable branches may have gravitational-wave signals. We leave these for future studies.

[1] B. P. Abbott *et al.* (LIGO Scientific and Virgo Collaborations), Phys. Rev. Lett. **116,** 061102 (2016).

[2] B. P. Abbott *et al.* (LIGO Scientific and VIRGO Collaborations), Phys. Rev. Lett. **118,** 221101 (2017); **121,** 129901(E) (2018).

[3] B. P. Abbott *et al.* (LIGO Scientific and Virgo Collaborations), Phys. Rev. X **9,** 031040 (2019).

[4] B. P. Abbott *et al.* (LIGO Scientific and Virgo Collaborations), Phys. Rev. Lett. **119,** 161101 (2017).

[5] B. P. Abbott *et al.* (LIGO Scientific and Virgo Collaborations), Phys. Rev. X **9,** 011001 (2019).

[6] B. Abbott *et al.* (LIGO Scientific and Virgo Collaborations), Astrophys. J. Lett. **892,** L3 (2020).

[7] R. Abbott *et al.* (LIGO Scientific and Virgo Collaborations), Astrophys. J. Lett. **896,** L44 (2020).

[8] M. Alford, M. Braby, M. W. Paris, and S. Reddy, Astrophys. J. **629,** 969 (2005).

[9] M. G. Alford, S. Han, and M. Prakash, Phys. Rev. D **88,** 083013 (2013).

[10] A. R. Bodmer, Phys. Rev. D **4,** 1601 (1971).

[11] E. Witten, Phys. Rev. D **30,** 272 (1984).

[12] H. Terazawa, Report No. INS-Report-336, INS, University of Tokyo, Tokyo, 1979.

[13] E. Farhi and R. L. Jaffe, Phys. Rev. D **30,** 2379 (1984).

[14] B. Holdom, J. Ren, and C. Zhang, Phys. Rev. Lett. **120,** 222001 (2018).

[15] P. Haensel, J. L. Zdunik, and R. Schaeffer, Astron. Astrophys. **160,** 121 (1986), https://inspirehep.net/literature/243725.

[16] C. Alcock, E. Farhi, and A. Olinto, Astrophys. J. **310,** 261 (1986).

[17] R. X. Xu, G. J. Qiao, and B. Zhang, Astrophys. J. Lett. **522,** L109 (1999).

[18] S. H. Yang, C. M. Pi, X. P. Zheng, and F. Weber, Universe **9,** 202 (2023).

[19] C. Zhang, Phys. Rev. D **101,** 043003 (2020).

[20] T. Zhao, W. Zheng, F. Wang, C. M. Li, Y. Yan, Y. F. Huang, and H. S. Zong, Phys. Rev. D **100,** 043018 (2019).

[21] J. Ren and C. Zhang, Phys. Rev. D **102,** 083003 (2020).

[22] Z. Cao, L. W. Chen, P. C. Chu, and Y. Zhou, Phys. Rev. D **106,** 083007 (2022).

[23] L. Wang, J. Hu, C. J. Xia, J. F. Xu, G. X. Peng, and R. X. Xu, Galaxies **9,** 70 (2021).

[24] W. L. Yuan, A. Li, Z. Miao, B. Zuo, and Z. Bai, Phys. Rev. D **105,** 123004 (2022).

[25] T. E. Restrepo, C. Providência, and M. B. Pinto, Phys. Rev. D **107,** 114015 (2023).

[26] C. J. Xia, S. S. Xue, R. X. Xu, and S. G. Zhou, Phys. Rev. D **101,** 103031 (2020).

[27] C. J. Xia, J. F. Xu, G. X. Peng, and R. X. Xu, Phys. Rev. D **106,** 034016 (2022).

[28] J. Ren and C. Zhang, Phys. Rev. D **108,** 063012 (2023).

[29] V. V. Usov, Phys. Rev. Lett. **80,** 230 (1998).

[30] N. K. Glendenning, C. Kettner, and F. Weber, Astrophys. J. **450,** 253 (1995).

[31] R. X. Xu and G. J. Qiao, Chin. Phys. Lett. **15,** 934 (1998).

[32] R. X. Xu, B. Zhang, and G. J. Qiao, Astropart. Phys. **15,** 101 (2001).

[33] A. Kuerban, J. J. Geng, Y. F. Huang, H. S. Zong, and H. Gong, Astrophys. J. **890,** 41 (2020).

[34] Ren-Xin Xu and Fei Wu, Chin. Phys. Lett. **20,** 806 (2003).

[35] F. Wu, R. X. Xu, and B. Q. Ma, J. Phys. G **33,** 597 (2007).

[36] P. Kankiewicz, M. Rybczynski, Z. Włodarczyk, and G. Wilk, Astrophys. J. **839,** 31 (2017).

[37] J. J. Geng, Y. F. Huang, and T. Lu, Astrophys. J. **804,** 21 (2015).

[38] Z. C. Zou, Y. F. Huang, and X. L. Zhang, Universe **8,** 442 (2022).

[39] X. Wang, A. Kuerban, J. J. Geng, F. Xu, X. L. Zhang, B. J. Zuo, W. L. Yuan, and Y. F. Huang, Phys. Rev. D **104,** 123028 (2021).

[40] J. J. Geng, B. Li, and Y. F. Huang, Innovation **2,** 100152 (2021).

[41] Y. Zhang, J. J. Geng, and Y. F. Huang, Astrophys. J. **858,** 88 (2018).

[42] Y. F. Huang and Y. B. Yu, Astrophys. J. **848,** 115 (2017).

[43] C. Zhang, Y. Luo, H. b. Li, L. Shao, and R. Xu, arXiv:2306.08234.

[44] E. P. Zhou, X. Zhou, and A. Li, Phys. Rev. D **97,** 083015 (2018).

[45] S. Weissenborn, I. Sagert, G. Pagliara, M. Hempel, and J. Schaffner-Bielich, Astrophys. J. Lett. **740,** L14 (2011).

[46] C. Zhang and R. B. Mann, Phys. Rev. D **103,** 063018 (2021).

[47] R. X. Xu, Astrophys. J. Lett. **596,** L59 (2003).

[48] X. Lai and R. Xu, J. Phys. Conf. Ser. **861,** 012027 (2017).

[49] Z. Q. Miao, C. J. Xia, X. Y. Lai, T. Maruyama, R. X. Xu, and E. P. Zhou, Int. J. Mod. Phys. E **31,** 2250037 (2022).

[50] X. Lai and R. Xu, Mon. Not. R. Astron. Soc. **398,** L31 (2009).

[51] Y. Gao, X. Y. Lai, L. Shao, and R. X. Xu, Mon. Not. R. Astron. Soc. **509,** 2758 (2021).

[52] X. Y. Lai, Y. W. Yu, E. P. Zhou, Y. Y. Li, and R. X. Xu, Res. Astron. Astrophys. **18,** 024 (2018).

[53] X. Y. Lai, C. J. Xia, Y. W. Yu, and R. X. Xu, Res. Astron. Astrophys. **21,** 250 (2021).

[54] X. Lai, E. Zhou, and R. Xu, Eur. Phys. J. A **55,** 60 (2019).

[55] E. P. Zhou, J. G. Lu, H. Tong, and R. X. Xu, Mon. Not. R. Astron. Soc. **443,** 2705 (2014).

[56] A. Z. Zhou, R. X. Xu, X. J. Wu, N. Wang, and X. Y. Hong, Astropart. Phys. **22,** 73 (2004).

[57] P. Demorest, T. Pennucci, S. Ransom, M. Roberts, and J. Hessels, Nature (London) **467,** 1081 (2010).

[58] C. Zhang, Y. Gao, C. J. Xia, and R. Xu, Phys. Rev. D **108,** 063002 (2023).

[59] C. Zhang, Phys. Rev. D **104,** 083032 (2021).

[60] C. Zhang, M. Gammon, and R. B. Mann, Phys. Rev. D **104,** 123007 (2021).

[61] D. Blaschke, E. O. Hanu, and S. Liebing, Phys. Rev. C **105,** 035804 (2022).

[62] D. Blaschke, U. Shukla, O. Ivanytskyi, and S. Liebing, Phys. Rev. D **107,** 063034 (2023).

[63] P. S. Koliogiannis, G. A. Tsalis, C. P. Panos, and C. C. Moustakidis, Phys. Rev. D **107,** 044069 (2023).

[64] P. T. Oikonomou and C. C. Moustakidis, Phys. Rev. D **108,** 063010 (2023).

[65] M. Gammon, S. Rourke, and R. B. Mann, arXiv:2309.00703.

[66] M. G. Alford, K. Rajagopal, and F. Wilczek, Nucl. Phys. **B537,** 443 (1999).

[67] K. Rajagopal and F. Wilczek, Phys. Rev. Lett. **86,** 3492 (2001).

[68] G. Lugones and J. E. Horvath, Phys. Rev. D **66,** 074017 (2002).

[69] M. Alford and K. Rajagopal, J. High Energy Phys. 06 (2002) 031.

[70] E. S. Fraga, R. D. Pisarski, and J. Schaffner-Bielich, Phys. Rev. D **63,** 121702 (2001).

[71] K. A. Olive *et al.* (Particle Data Group), Chin. Phys. C **38,** 090001 (2014).

[72] J. P. Pereira, C. V. Flores, and G. Lugones, Astrophys. J. **860,** 12 (2018).

[73] G. Lugones and A. G. Grunfeld, Universe **7,** 493 (2021).

[74] J. E. Lennard and I. Jones, Proc. R. Soc. A **106,** 441 (1924).

[75] R. C. Tolman, Phys. Rev. **55,** 364 (1939).

[76] J. R. Oppenheimer and G. M. Volkoff, Phys. Rev. **55,** 374 (1939).

[77] A. E. H. Love, Proc. R. Soc. A **82,** 73 (1909).

[78] T. Hinderer, Astrophys. J. **677,** 1216 (2008).

[79] T. Hinderer, B. D. Lackey, R. N. Lang, and J. S. Read, Phys. Rev. D **81,** 123016 (2010).

[80] S. Postnikov, M. Prakash, and J. M. Lattimer, Phys. Rev. D **82,** 024016 (2010).

[81] T. Damour and A. Nagar, Phys. Rev. D **80,** 084035 (2009).

[82] J. Takatsy and P. Kovacs, Phys. Rev. D **102,** 028501 (2020).

[83] M. C. Miller *et al.*, Astrophys. J. **887,** L24 (2019).

[84] T. E. Riley *et al.*, Astrophys. J. **887,** L21 (2019).

[85] M. C. Miller *et al.*, Astrophys. J. **918,** L28 (2021).

[86] T. E. Riley *et al.*, Astrophys. J. **918,** L27 (2021).

[87] K. Schertler, S. Leupold, and J. Schaffner-Bielich, Phys. Rev. C **60,** 025801 (1999).

[88] X. Y. Lai, C. A. Yun, J. G. Lu, G. L. Lü, Z. J. Wang, and R. X. Xu, Mon. Not. R. Astron. Soc. **476,** 3303 (2018).

[89] W. Wang, X. Lai, E. Zhou, J. Lu, X. Zheng, and R. Xu, Mon. Not. R. Astron. Soc. **500,** 5336 (2020).

[90] X. Y. Lai, W. H. Wang, J. P. Yuan, R. P. Lu, H. Yue, and R. X. Xu, Mon. Not. R. Astron. Soc. **523,** 3967 (2023).

[91] R. Lu, H. Yue, X. Lai, W. Wang, S. Zhang, and R. Xu, Mon. Not. R. Astron. Soc. **520,** 4289 (2023).

[92] R. Anglani, R. Casalbuoni, M. Ciminale, N. Ippolito, R. Gatto, M. Mannarelli, and M. Ruggieri, Rev. Mod. Phys. **86,** 509 (2014).

[93] L. M. Lin, Phys. Rev. D **88,** 124002 (2013).

[94] M. Mannarelli, G. Pagliaroli, A. Parisi, and L. Pilo, Phys. Rev. D **89,** 103014 (2014).

[95] M. Mannarelli, G. Pagliaroli, A. Parisi, L. Pilo, and F. Tonelli, Astrophys. J. **815,** 81 (2015).

[96] C. V. Flores and G. Lugones, Classical Quantum Gravity **31,** 155002 (2014).

[97] I. F. Ranea-Sandoval, O. M. Guilera, M. Mariani, and M. G. Orsaria, J. Cosmol. Astropart. Phys. 12 (2018) 031.

[98] C. Constantinou, S. Han, P. Jaikumar, and M. Prakash, Phys. Rev. D **104,** 123032 (2021).

[99] C. Constantinou, T. Zhao, S. Han, and M. Prakash, Phys. Rev. D **107,** 074013 (2023).

[100] T. Zhao, C. Constantinou, P. Jaikumar, and M. Prakash, Phys. Rev. D **105,** 103025 (2022).

[101] S. Y. Lau and K. Yagi, Phys. Rev. D **103,** 063015 (2021).

[102] J. Zhu, C. Wang, C. Xia, E. Zhou, and Y. Ma, Phys. Rev. D **107,** 083023 (2023).